J Mater Sci (2008) 43:6029–6037
DOI 10.1007/s10853-008-2954-x

Detailed investigation of ultrasonic Al–Cu wire-bonds: I. Intermetallic formation in the as-bonded state

M. Drozdov · G. Gur · Z. Atzmon · Wayne D. Kaplan

Received: 9 July 2008 / Accepted: 14 August 2008 / Published online: 4 September 2008
© Springer Science+Business Media, LLC 2008

Abstract Scanning and transmission electron microscopy were used to study intermetallic formation and the interface morphology in copper wire-bonds. The ends of copper wires were melted in air and in a protective environment to form wire-balls. The protective environment enabled formation of symmetrical and relatively defect-free copper balls, together with a smaller heat affected zone (in comparison with wires melted in air). Detailed morphological and compositional characterization of the Al–Cu as-bonded interface was conducted using scanning and transmission electron microscopy, on specimens prepared by focused ion beam milling. Discontinuous and non-uniform intermetallics were found in regions where high localized stress was introduced during the wire-bonding process. The main intermetallic phase was found to be Al_2Cu.

Introduction

Wire-bonding is one of the main technologies used for electronic chip interconnections. In the process of bonding the wire to the metallization pad and to the lead, a reliable bond with good adhesion is needed. This is achieved by applying ultrasonic and thermal energies that assist the bonding process (see Fig. 1) [1].

M. Drozdov · W. D. Kaplan (✉)
Department of Materials Engineering, Technion—Israel Institute of Technology, Haifa 32000, Israel
e-mail: kaplan@tx.technion.ac.il

G. Gur · Z. Atzmon
Kulicke & Soffa Bonding Tools, Yokneam Elite, Israel

One of the initial stages of the wire-bonding process is the melting of a wire tip by an electrical spark to form a free air ball (FAB) (Fig. 1). Melting of the wire is done to form a symmetrical ball that will be bonded to the (aluminum) metallization. Non-symmetrical FABs may cause short circuits, thus it is important to control the shape of the FAB. During melting, as a result of heat transfer from the ball tip, part of the wire located adjacent to the FAB is exposed to elevated temperatures. This part of the wire goes through annealing and is referred to as the heat-affected zone (HAZ). This zone has a larger grain size and lower hardness in comparison to the rest of the wire. Thus the HAZ is weaker than the rest of the wire and is prone to failure. A shorter HAZ with a smaller grain size can increase the bond reliability [1].

The mechanical properties of joins between two different metals are strongly affected by the presence of intermetallic phases. These phases can ensure direct connection and a strong uniform bond between the metals. However, intermetallic phases may also have lower electrical and thermal conductivity, thus damaging the chip-package electrical connection [2]. Therefore, a study of the intermetallic phases formed at the Al–Cu interface during the wire-bonding process is crucial for understanding the process.

It should be noted that while the presence of intermetallic phases indicates that an intimate contact occurred at the interface, it is not an obligatory condition for bonding. Bonding means physical–chemical bonds formed at the interface, which is facilitated by charge transfer. Therefore, bonding can occur between two completely immiscible solids without the formation of secondary phases. For example, charge transfer at metal–oxide interfaces results in a measurable mechanical work of adhesion without the formation of intermediate phases at the interface [3, 4].

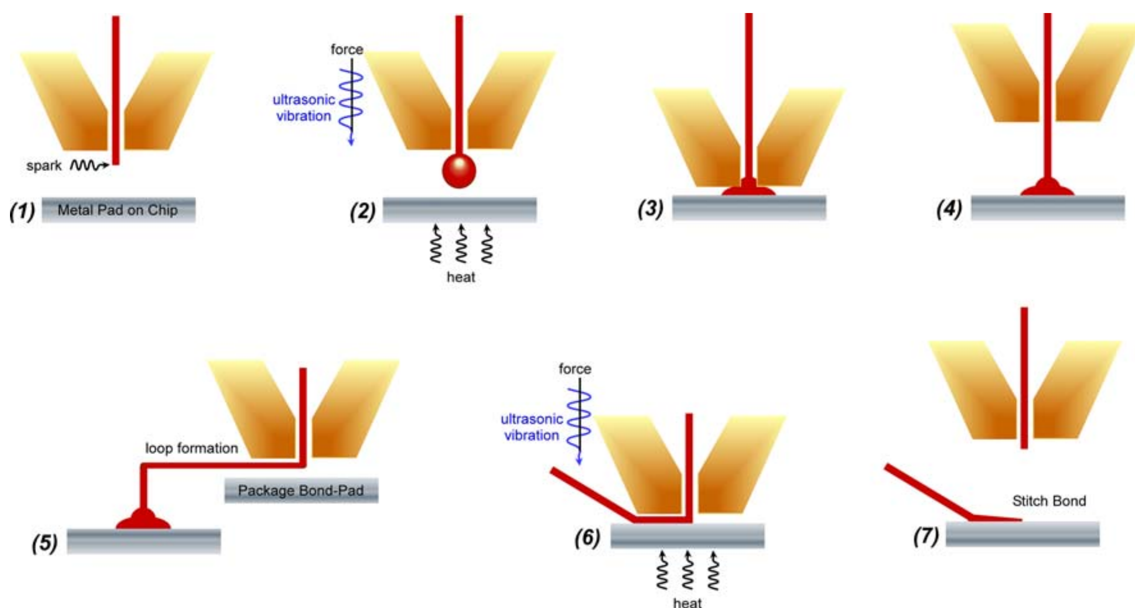

Fig. 1 Schematic illustration of the wire-bonding process, redrawn after [1]

Usually, gold wires are used in advanced wire-bonding processes. Due to their lower cost, superior thermal and electrical conductivity and higher metallurgical stability, copper wires are currently being evaluated as a substitute for gold. In order to incorporate copper wires into the packaging industry, an understanding of Al–Cu bond formation is essential. Methods currently in use to analyze Al–Cu wire-bonds include microstructural characterization and hardness measurements of the copper wire after formation of the FAB; evaluation of the damage introduced into the Al metallization and the Si substrate during the bonding process; evaluation of the adhesion strength of the bond; estimation of the actual bonded area of the wire-bond and examination of Al–Cu intermetallic phase formation after heat treatments; and comparison of all of the above with Al–Au wire-bonds. The copper wires are usually examined by optical microscopy (OM) and scanning electron microscopy (SEM). The morphology of the Al–Cu interface is examined normally by OM and SEM, while the intermetallic composition is evaluated via energy dispersive spectroscopy (EDS) mounted on SEM, as well as X-ray diffraction (XRD) [5–13].

The resolution achieved by OM and SEM-EDS is *insufficient* for detailed morphological and compositional analysis of the Al–Cu interface of wire-bonded specimens [14]. This may be the reason for the fact that studies conducted on Al–Cu wire-bonds repeatedly report that no intermetallics are found at the as-bonded Al–Cu interface [11, 15–17].

In this research, the as-bonded interface was characterized by transmission electron microscopy (TEM), TEM-EDS and energy filtered (EF) TEM, while site-specific and relatively artifact-free specimen preparation was carried out using a dual-beam focused ion beam (FIB). The channeling effect of ion-induced secondary electrons (SE) in FIB was used for qualitative grain size measurements of the copper wires before and after the bonding process. In a companion paper, the microstructural evolution of *annealed* Al–Cu wire-bonds is reported [18].

Experimental methods

Specimen preparation

Free air balls

A 25.4 μm diameter Cu wire of 99.99% purity (4 N) was used to prepare FABs. Two sets of FABs were examined; one set was prepared using an electric spark, as is commonly done in wire-bonding, in a reducing environment composed of 95% N_2 and 5% H_2 (forming gas); and another set was prepared by forming the copper FAB in air. The flow rate of the forming gas was optimized to obtain symmetric FABs [19]. The electric spark used to melt the wires was based on 40 mA for 0.7 ms across a gap of 0.76 mm, for FABs prepared in both air and forming gas. The FAB specimens were prepared for microstructural investigations in cross-section using a dual-beam FIB (FEI Strata 400S).

Al–Cu reference specimen

In order to evaluate possible damage introduced into the Al–Cu interface during FIB specimen preparation, a

reference specimen consisting of a thin Al layer capped with a thin Cu layer was prepared by physical vapor deposition (PVD) (Von Ardenne sputtering system, model NS320S). During the sputtering process the chamber was filled with argon at a pressure of 6.3 m Torr (for Al deposition) and 5 m Torr (for Cu deposition). In order to avoid oxidation of the aluminum layer, copper deposition was conducted immediately after the aluminum deposition without breaking vacuum. Reference TEM specimens were prepared using the FIB in a manner similar to preparation of the as-bonded wire-bonded specimens, as explained in the next section.

Al–Cu wire-bonds

Si wafers coated with a uniform Al metallization on top of thermally grown SiO_2 were used for the ball bonding process. The nominal thickness of the Al metallization was 800 nm. The Al metallization consisted of 0.5 wt.% Cu and 1 wt.% Si. A 25.4 μm diameter Cu wire of 99.99% purity (4 N), identical to the wires used for the FAB investigations, was used for ball bonding. The ball bonding was performed on a K&S model 8028 PPS automatic wire bonder, using a capillary with an inner chamfer angle of 90° (ICA 90). The ball bond diameter was kept within 52 ± 3 μm. Thermosonic ball bonding of each Si die was performed at 220 °C for an approximate time of 18 s per device (approximately 0.2 s per bond) with a pre- and post-heat for 18 s at 150 °C. The bonding parameters were optimized to ensure zero pad peals, and the resulting average bond shear force was 13.3 kg/mm^2, which corresponds to an optimal shear strength of as-bonded Al–Au wire-bonds (14–15.5 kg/mm^2) [17]. Melting of the Cu wire tip to prepare a FAB was conducted in a reducing atmosphere (95%N_2, 5%H_2).

Transmission electron microscopy specimens were prepared using a dual-beam FIB, while specimen examination during the preparation was carried out by SEM and (at the final stages of the preparation) by scanning transmission electron microscopy (STEM) in the FIB. During specimen preparation, gallium ions entered the specimen at 30 kV in a direction parallel to the examined interface, while the specimen cleaning routine was carried out at 2–5 kV at an incident angle of 5–7° to the TEM specimen [20].

Characterization

Micrometer length-scale characterization of the FABs and of the copper bonds was conducted using SEs under a scanning incident electron beam in the FIB. Characterization of the copper grain morphology of FABs and wire-bonded cross-sections was conducted using the channeling effect in both SEM and FIB.

The channeling effect occurs when an incident ion or electron beam is aligned parallel to a low-index zone axis of the crystalline sample. Under these conditions, the beam does not collide with target atoms near the surface, but rather penetrates deeper into the sample. When an inelastic collision occurs, the SEs emitted from the “channeled” grain have a smaller probability of escaping to the surface, thus these grains appear darker than unaligned grains, or grains aligned parallel to a higher index zone axes [21–25].

Measurements of the HAZ after FAB preparation were conducted by counting the number of Cu grains per copper wire thickness. The micrographs used for counting were acquired by FIB in the ion-induced SE mode. The Al–Cu intermetallic grain size was measured from micrographs obtained by TEM.

Initial characterization of the copper bonds was conducted using SEs in SEM mode of the dual-beam FIB, and subsequently an immersed-lens mode of SE acquisition was used for better spatial resolution.

Scanning transmission electron microscopy mounted on the dual-beam FIB was used for initial characterization of the TEM specimens. This provided qualitative information on the thickness of the TEM specimens during thinning, and initial morphological characterization of the specimens.

Extensive morphological characterization of the Al–Cu bonds was carried out using TEM on a number of different instruments: JEOL 3010UHR (ultra high resolution) TEM, FEI Tecnai G^2 F20 field emission gun (FEG)-TEM with a high angle annular dark field (HAADF) STEM detector and a retractable EDAX detector; FEI Tecnai G^2 20 with a retractable EDAX detector, and the FEI Titan 80–300 kV monochromated and aberration corrected FEG-S/TEM.

In order to obtain as much information as possible regarding Al–Cu intermetallic formation at the wire-bonded interface, TEM specimens were prepared from both central and peripheral regions of the examined bonds. The “central” or “peripheral” region relates to a region located within 10 μm from the center of the bond, or 10 μm from the edge of a bond, respectively.

Compositional analysis

In order to obtain reliable information regarding the Al–Cu interface composition, the as-bonded interfaces were studied using EDS, and selected area diffraction (SAD) to confirm the crystal structure of the phases. Energy filtered TEM (EFTEM) was also used as a complimentary technique for compositional analysis.

Energy dispersive spectroscopy analysis was done on the FEI Tecnai F20 and Tecnai T20 microscopes, using the standardless procedure. In order to ensure acquisition of the signal from a selected region, the specimen was tilted 15° towards the EDS detector. The nominal beam diameters

used for the EDS analysis in Tecnai F20 and in Tecnai T20 were 0.65 and 1.6 nm, respectively.

Selected area diffraction patterns were acquired from the intermetallic grains found adjacent to the interface region, which were also characterized by TEM-EDS. The diffraction patterns were acquired using the Tecnai T20 TEM.

In EFTEM the electrons transmitted from the specimen are separated according to their energy loss due to elastic and inelastic interaction with the specimen. Due to the high sensitivity of the technique, it allows for acquisition of elemental maps in small time periods (up to 1 min), enabling a relatively high spatial resolution. The elemental maps presented in this research were obtained on the Titan 80–300 kV FEG-S/TEM using a Gatan GIF 866 Tridiem ERS EFTEM.

Results

Free air balls

During melting of the copper wire tip in a non-protective environment, oxidation of the wire occurs. As can be seen from Fig. 2, oxidation of the copper wire results in asymmetrical ball formation, voids, and flaws.

The copper FABs formed in a reducing atmosphere have a uniform shape. No asymmetries or flaws of the FABs were detected (Fig. 3).

During melting of the copper wire by an electrical spark, a large amount of energy is transferred into the wire. The thermal energy escapes by convection, radiation, and conduction via the wire above the melted tip, creating the HAZ. In order to understand the influence of the bonding environment on HAZ evolution, the HAZs of FABs produced in air and in a reducing environment were examined. The measured HAZ length for FABs melted in air was 98 ± 19 μm, while that in a reducing environment was 46 ± 4 μm. Figure 4 presents cross-sections of representative FABs formed in air and in a reducing environment. The HAZ length for FABs formed in air is up to twice as large as that of the FABs formed in a reducing environment.

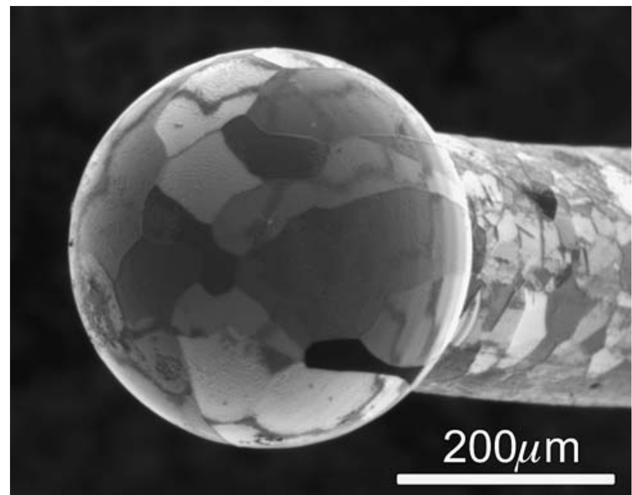

Fig. 3 SE FIB micrograph of a representative copper FAB produced in a reducing atmosphere. The FAB is completely symmetric with no visible flaws

As-bonded Al–Cu wire-bonds

Figure 5 presents SEM and ion-induced (FIB) SE micrographs of an as-bonded wire cross-section, which show that in the bond periphery the copper grains are smaller, while at the center of the bond they were larger. The copper grains at the periphery are elongated and aligned parallel to the Al metallization, while the copper grains at the center of the bond are more isotropic in shape. Smaller copper grains at the very center of the bond adjacent to the Al–Cu interface can also be detected in the FIB micrograph (Fig. 5b). The aluminum metallization thickness is not uniform at the very center of the bond, and at the bond periphery the aluminum layer is thinner than in other regions. No intermetallics can be detected in these micrographs.

Figure 6 presents a higher magnification SE SEM micrograph taken from the peripheral region of an as-bonded wire-bond. Voids forming a discontinuous void-line are detected closer to the bond periphery. A region composed of intermetallic (IM) grains is indicated. The presence of IM grains was confirmed by TEM analysis (see below). No intermetallics at the center of the bond were detected by SE SEM.

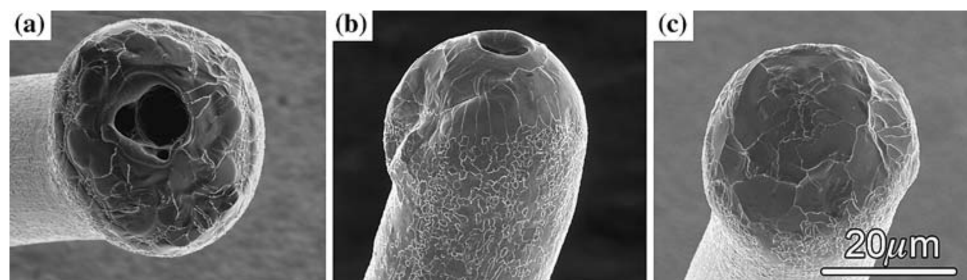

Fig. 2 Secondary electron (SE) SEM micrographs of copper free air balls produced in air. The scale bar is equivalent for all three micrographs

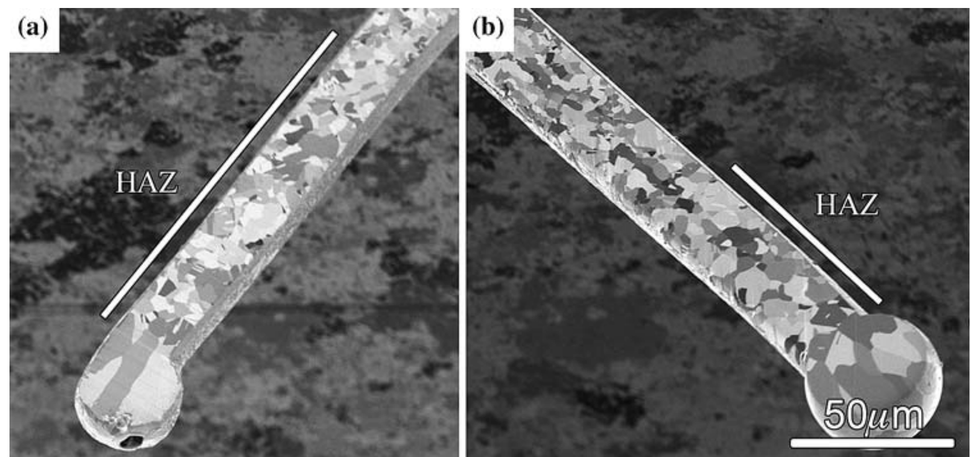

Fig. 4 SE FIB micrographs of representative FABs formed (**a**) in air and (**b**) in a protective environment. The heat-affected zone of the FABs produced in air is twice as large as that of FABs produced in a reducing environment. The scale bar is equivalent for both micrographs

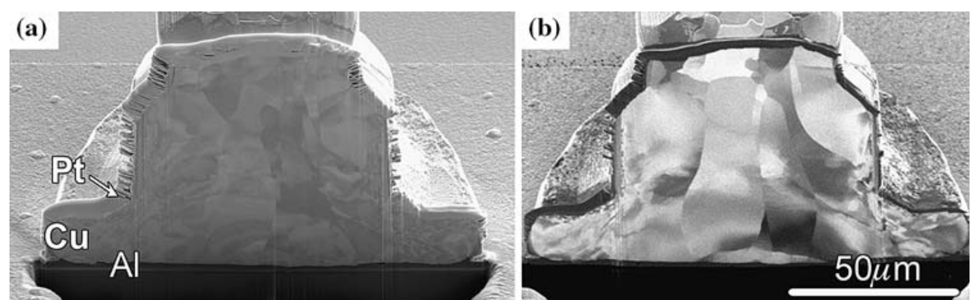

Fig. 5 (**a**) SE SEM micrograph and (**b**) SE FIB micrograph of the cross-section of an as-bonded wire-bond

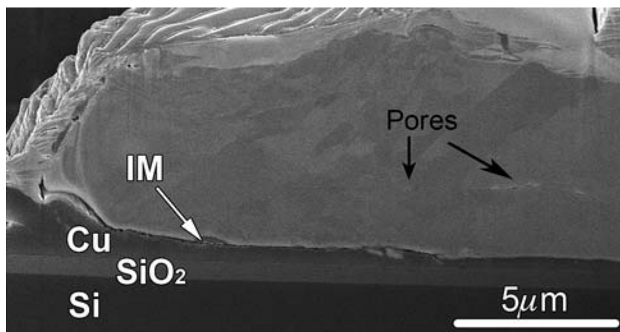

Fig. 6 SE SEM micrograph taken from the periphery of the as-bonded Al–Cu wire-bond

Figure 7 presents a HAADF STEM micrograph acquired from the intermetallic region indicated (by IM) in Fig. 6. The investigated intermetallic region consists of two different regions. Region 1 is richer in copper, has a brighter contrast and is located adjacent to the copper ball. Region 2 is located adjacent to the void and contains less copper. At the center of the second region, a grain with a different contrast is visible. The composition of this grain is similar to that of the aluminum metallization. The Cu to Al concentration ratios of the regions annotated in Fig. 6 are presented in Table 1.

Figure 8 is a bright field (BF) STEM micrograph of the central region of an as-bonded Al–Cu wire-bond. Larger and more uniform intermetallic grains are found at the Al–Cu interface in this region, than at the bond periphery. The composition of the intermetallic grains (measured by EDS) is presented in Table 2. The measured compositions do not correlate to a specific Al–Cu intermetallic phase.

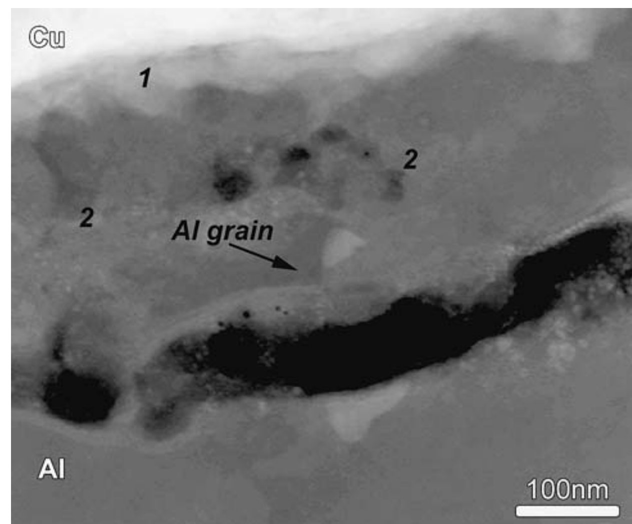

Fig. 7 HAADF-STEM micrograph acquired from the periphery of an as-bonded specimen. The STEM-EDS results of the annotated regions are presented in Table 1

The central region of another as-bonded Al–Cu specimen is presented in Fig. 9. An EFTEM map (Fig. 9b) provides information regarding the presence of aluminum

Table 1 The Cu to Al concentration ration, as measured by STEM-EDS in the regions noted in Fig. 7

	Cu (at.%, relative to Al) (%)
Region 1	37 ± 1.5
Region 2[a]	13.5 ± 2.5
Al grain	1.5 ± 0.5

[a] Region 2 was also found to be rich in oxygen

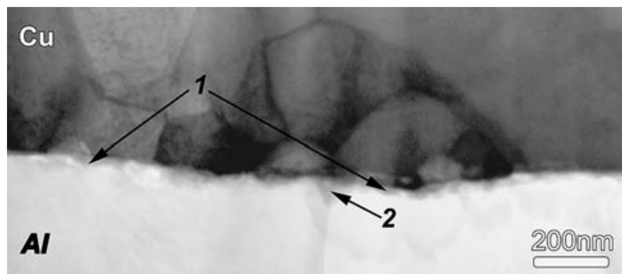

Fig. 8 BF STEM micrograph taken from the center of an as-bonded Al–Cu wire-bond. The STEM-EDS results of the annotated regions are given in Table 2

Table 2 The Cu to Al concentration ratios, as measured by STEM-EDS from the regions noted in Fig. 8

	Cu (at.%, relative to Al) (%)
Region 1	64 ± 2
Region 2	44 ± 1.5

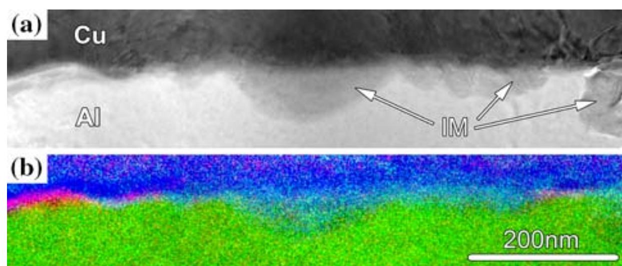

Fig. 9 (**a**) BF TEM and (**b**) EFTEM micrographs taken from the center of an as-bonded Al–Cu wire-bond. The colors in the EFTEM micrograph correlate to aluminum K-edge (green), oxygen K-edge (red), and copper L-edge (blue). The scale bar is equivalent for both micrographs

(marked by green) oxygen (red), and copper (blue). The intermetallic regions indicated (by IM) in the BF TEM micrograph (Fig. 9a) were also found to contain copper (blue-green regions in the aluminum layer) by EFTEM (Fig. 9b). Oxygen (indicated in red in the EFTEM micrograph) was found at voids at the Al–Cu interface.

Another central region of an as-bonded wire-bond is presented in Fig. 10. An EFTEM map (Fig. 10b) provides information regarding the presence of oxygen (marked by red), aluminum (green), and copper (blue), and clearly indicates the existence of oxygen at the interface. Intermetallic grains were detected and are indicated as 1 and 2 in Fig. 10a. The composition of the intermetallic grains noted in Fig. 10a was examined by STEM-EDS (Table 3) and their structure was confirmed by SAD (Fig. 10c and d, respectively). The SAD patterns of the grains indicated in Fig. 10a confirmed the presence of Al_2Cu. Whereas most of the intermetallic grains are found at the Al–Cu interface, grain 1 noted in Fig. 10a was found in the aluminum metallization region, at an aluminum grain boundary.

Al–Cu reference specimen

Figure 11 presents a BF STEM micrograph of the reference specimen that consists of aluminum and copper layers produced by PVD sputtering. The TEM specimen was prepared by FIB, using identical working conditions to the TEM specimens prepared from the wire-bonds. No intermetallic phase is visible at the Al–Cu interface.

Discussion

Free air balls

Free air ball formation is a very important step in the wire-bonding process. FABs with asymmetric shapes or varying size, which form due to oxidation and the formation of oxide scales in a non-protective environment, may cause stress concentrations in the bonded area, and in some cases, when the FAB is too small, direct contact between the capillary and the Al metallization. Moreover, asymmetric ball-bonds may result in contact between individual wires, leading to an electrical short.

After FAB formation, energy transmitted to the wire tip is removed from the FAB by conduction (through the wire), convection, and radiation. The heat transfer coefficient for conduction via the wire is constant regardless of the environment. As such, the total heat flux through the wire depends only on the residual thermal energy in the FAB, after convection and radiation to the environment. Heat transfer via radiation is two orders of magnitude lower than by conduction and convection, and thus can be disregarded [26]. During melting of the copper wire tip in a reducing atmosphere (95%N_2 and 5%H_2) the reducing gas flows over the wire tip with a relatively low velocity. The thermal conductivity coefficient of air at 300 K is lower than that of the reducing atmosphere; 26.2 MW/mK for air and 34 MW/mK for the reducing atmosphere [27]. As such, regardless of the inert gas flow, more energy is transferred via convection and less by conduction via the

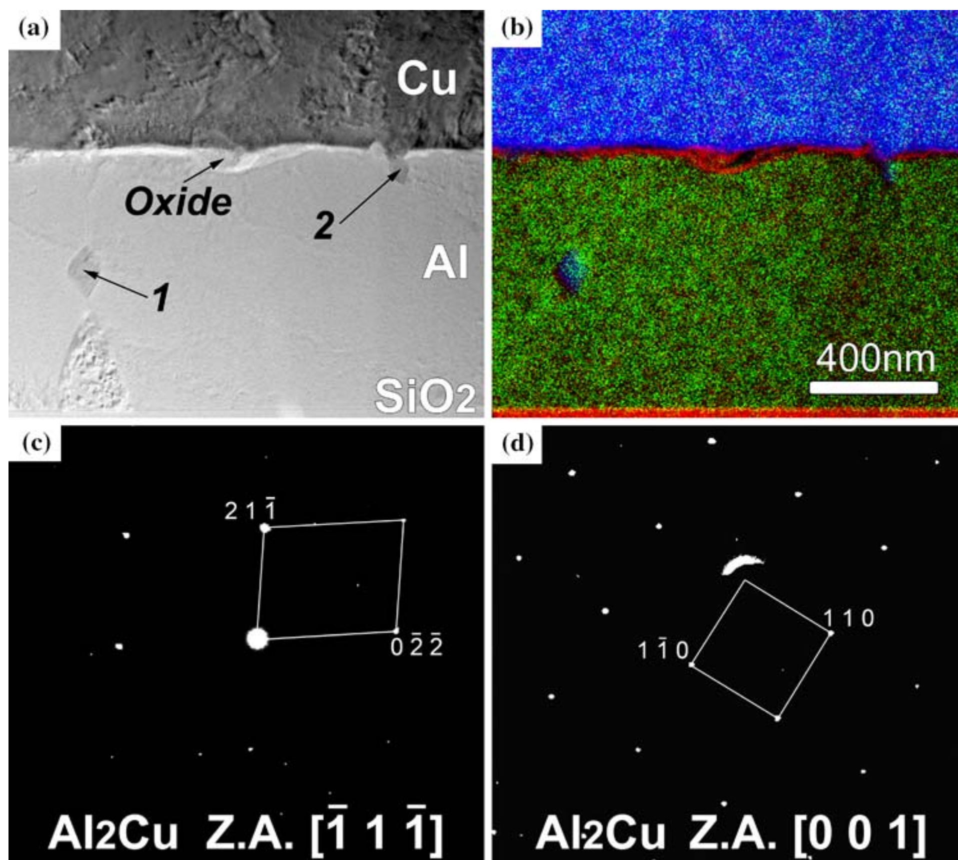

Fig. 10 (**a**) BF TEM and (**b**) EFTEM micrographs taken from the center of an as-bonded Al–Cu wire-bond. The STEM-EDS results of the annotated regions are indicated in Table 3. The colors at the EFTEM micrograph correlate to oxygen (red), aluminum (green) and copper (blue) atoms. The scale bar is equivalent for both micrographs. SAD patterns of the grain marked as 1 and the grain marked as 2 noted in (**a**) are given in (**c**) and (**d**), respectively. The central beam in the SAD in (**d**) is blanked to emphasize the diffracted beams

Table 3 The Cu to Al concentration ratios, as measured by STEM-EDS from the regions noted in Fig. 10a

	Cu (at.%, relative to Al) (%)
Grain 1	25 ± 5
Grain 2	24 ± 1

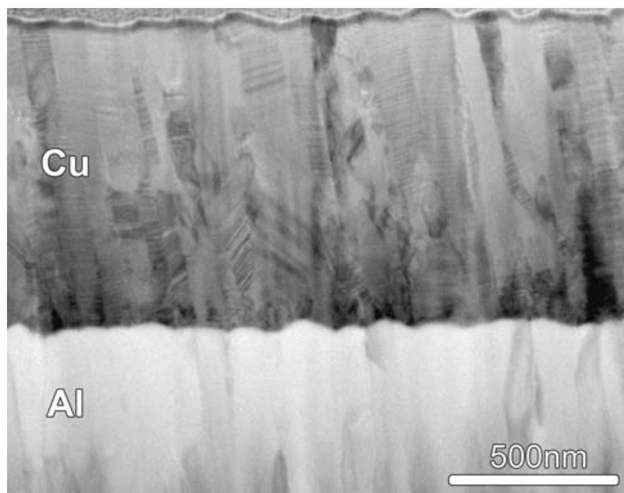

Fig. 11 BF STEM micrograph of an Al–Cu interface obtained from a reference specimen prepared by PVD. The TEM specimen was prepared by FIB. No intermetallics were found at the Al–Cu interface

wire during FAB formation in an inert atmosphere. Flow of the inert gas around the copper FAB also increases the heat transfer by convection. Since less energy is transferred via the wire, smaller HAZ lengths for FABs formed in an inert atmosphere were observed.

Being a highly oxidative metal, copper oxidizes during FAB formation in air. Copper oxidation into Cu_2O is an exothermic process ($\Delta H = -167.5 \pm 4$ kJ/mol) [28]. The heat, which is emitted during the oxidation process, contributes to the total thermal energy transferred into the HAZ and to the HAZ growth.

As-bonded Al–Cu wire-bonds

According to finite element analysis of wire-bonds formed using a capillary with ICA 90, the bond periphery sustains the largest applied mechanical stress during the bonding process, while the bond center sustains the smallest applied stress during the bonding process [15]. However, smaller copper grains elongated parallel to the Al–Cu interface were found at the bond center (see Fig. 5). This local morphology may be created during the initial contact and deformation of the copper FAB with the aluminum metallization (which occurs at the bond center), followed by recrystallization due to thermal/ultrasonic activation. The

smaller elongated copper grains may also originate from deformation induced by the ultrasonic motion after contact of the FAB with the Al metallization, which dominates the evolving microstructure in the absence of mechanical stress.

Despite consistent reports of no intermetallic formation during the Al–Cu wire-bonding process, intermetallics at the Al–Cu interface were detected for the as-bonded samples. The detected intermetallics were discontinuous and found at the periphery of the bond, as well as at the bond center.

The structure of the intermetallic grains found at the bond periphery suggests that intermetallic formation occurred during application of combined mechanical and ultrasonic forces. Thus incorporation of an aluminum grain into the intermetallic region, as seen in Fig. 7, can also be explained. Smaller intermetallic grains found in the periphery region (relative to the intermetallic grains found at the bond center) also suggest that extensive mechanical stress was applied during intermetallic formation at the bond edge. Oxygen found in the intermetallic regions at the bond periphery correlates with the increased porosity of the IM region. The intermetallic grain detected in the aluminum region (Fig. 10) suggest that for the as-bonded Al–Cu wire-bonds, intermetallic growth *may* occur by grain boundary diffusion. Alternatively, this specific intermetallic grain may have formed during the metallization process due to the presence of Cu in the metallization alloy.

The composition of the intermetallics as measured by STEM-EDS at the bond center differs from that found at the bond periphery; more copper-rich intermetallics were found at the bond center. However, the examined intermetallic grains are relatively small, and the STEM-EDS measurements could be influenced by nearby grains, decreasing the accuracy of the measurements. Tilt of the specimen towards the detector introduced additional errors into the EDS measurement. However, SAD patterns taken from the intermetallic grains located at the bond center confirm the presence of the Al_2Cu intermetallic phase.

Al–Cu reference specimen

During specimen preparation by FIB heating of the region subjected to the ion milling might occur. Regardless of the fact that in highly conductive specimens the heating probably does not exceed 10 K above the ambient temperature [29], the influence of Ga ions on intermetallic formation at the Al–Cu couple should be understood. The fact that no intermetallics were found at the Al–Cu interface (see Fig. 11) allows us to believe that specimen preparation using FIB in the current research is not the source for intermetallic formation.

Summary and conclusions

The purpose of this research was to understand the microstructure of as-bonded Al–Cu wire-bonds. In order to achieve this, both FAB formation and the Al–Cu wire-bonds were studied. Due to the length-scales of the microstructure involved, high resolution microscopy techniques were used.

Free air balls produced in a reducing gas were found to be uniform in shape and flawless, in contrast to the FABs produced in air. Moreover, it was found that due to the higher heat transmittance of the reducing gas (that consists of 95 wt.% N_2 and 5 wt.% H_2) in comparison with air, and to the energy emitted during the copper oxidation (during the FAB production in air) the length of the HAZ in copper wires melted in a reducing atmosphere is shorter than the HAZ of copper wires processed in air. This is important, since a shorter HAZ is associated with a higher mechanical stability of the copper ball-bond.

Analysis of the bonded copper grains revealed smaller copper grains at the periphery of the bond, in a region where the highest mechanical stresses were applied during the bonding process. Smaller copper grains were also found at the center of copper balls, presumably due to plastic deformation and recrystallization during initial contact of the FAB with the substrate.

As opposed to the data available in the literature, intermetallics *were* found in as-bonded specimens. The intermetallics formed were discontinuous and were found adjacent to smaller copper grains, i.e., in regions subjected to higher stress. This indicates that localized stresses incorporated into the Al–Cu interfacial region during the bonding process catalyze intermetallic formation. The intermetallics found at the Al–Cu interface were identified as Al_2Cu.

Acknowledgements The authors thank A. Berner, Y. Kauffman, and I. Popov for fruitful discussions. This research was partially supported by the Russell Berrie Nanotechnology Institute at the Technion.

References

1. Harman G (1997) Wire bonding in microelectronics materials, processes, reliability and yield. McGraw-Hill
2. Braunovic M, Alexandrov N (1994) IEEE Trans Compon Hybr Manuf Technol A 17(1):78. doi:10.1109/95.296372
3. Brydson R, Bruley J, Mullejans H, Scheu C, Ruhle M (1995) Ultramicroscopy 59(1–4):81. doi:10.1016/0304-3991(95)00020-2
4. Sadan H, Kaplan WD (2006) J Mater Sci 41(16):5099. doi:10.1007/s10853-006-0437-5
5. Toyozawa K, Fujita K, Minamide S, Maeda T (1990) IEEE Trans Compon Hybr Manuf Technol 13(4):667. doi:10.1109/33.62577
6. Singh I, On JY, Levine L (2005) Proc Electron Compon Technol 55(1):843

7. Tan CW, Daud AR (2002) J Mater Sci Mater Electron 13(5):309. doi:10.1023/A:1015580227090
8. Murali S, Srikanth N, Vath CJ (2003) Mater Charact 50(1):39. doi:10.1016/S1044-5803(03)00102-5
9. Wulff FW, Breach CD, Saraswati SD, Dittmer KJ (2004) Proc Electron Packag Technol Conf 348:353
10. Onuki J, Koizumi M, Araki I (1987) IEEE Trans Compon Hybr Manuf Technol 10(4):550. doi:10.1109/TCHMT.1987.1134799
11. Ratchev P, Stoukatch S, Swinnen B (2006) Microelectron Reliab 46(8):1315. doi:10.1016/j.microrel.2005.11.002
12. Kim H-J, Lee JY, Paik K-W, Koh K-W et al (2003) IEEE Trans Compon Packag Tech 26(2):367. doi:10.1109/TCAPT.2003.815121
13. Murali S, Srikanth N, Wong YM, Vath CJ (2007) J Mater Sci 42(2):615. doi:10.1007/s10853-006-1148-7
14. Karpel A, Gur G, Atzmon Z, Kaplan WD (2007) J Mater Sci 42(7):2334. doi:10.1007/s10853-007-1592-z
15. Wulff FW, Breach CD, Saraswati SD, Dittmer KJ, Garnier M (2005) www.kns.com. Accessed 30 August 2007
16. Murali S, Srikanth N, Vath CJ III (2003) Mater Res Bull 38(4):637. doi:10.1016/S0025-5408(03)00004-7
17. Murali S, Srikanth N, Vath CJ (2006) J Electron Packag 128(3):192. doi:10.1115/1.2229214
18. Drozdov M, Gur G, Atzmon Z, Kaplan WD (2008) J Mater Sci. doi:10.1007/s10853-008-2955-9
19. Zhong ZW, Ho HM, Tan YC, Tan WC et al (2007) Microelectron Eng 84(2):368. doi:10.1016/j.mee.2006.11.003
20. Thangadurai P, Lumelsky Y, Silverstein MS, Kaplan WD (2008) Mater Char. doi:10.1016/j.matchar.2008.02.007 (in press)
21. Wang G, Wu SD, Esling C, Li GY et al (2003) Adv Eng Mater 5(8):593. doi:10.1002/adem.200300388
22. Wang G, Wu SD, Zuo L, Esling C et al (2003) Mater Sci Eng A 346(1–2):83. doi:10.1016/S0921-5093(02)00521-X
23. Kempshall BW, Schwarz SM, Prenitzer BI, Giannuzzi LA et al (2001) J Vac Sci Technol B 19(3):749. doi:10.1116/1.1368670
24. Casey JD, Phaneuf M, Chandler C, Megorden M et al (2002) J Vac Sci Technol B 20(6):2682. doi:10.1116/1.1521736
25. Karpel A, Gur G, Atzmon Z, Kaplan WD (2007) J Mater Sci 42(7):2347. doi:10.1007/s10853-007-1593-y
26. Cohen IM, Huang LJ, Ayyaswamy PS (1995) Int J Heat Mass Transfer 38(9):1647. doi:10.1016/0017-9310(94)00294-6
27. CRC handbook of chemistry and physics, 87th edn. http://www.hbcpnetbase.com/. Accessed 30 August 2007
28. Smithells CF (1976) Metals reference book. London & Boston, Butterworths
29. Campisano SU, Chu T, Cannavo S, Rimini E (1984) Mater Res Society Symp Pros 97:102